Particle sizing with a fast polar nephelometer

Jean-Luc Castagner and Irving J. Bigio

We reported previously the design of a polar nephelometer that uses a rotational confocal imaging setup to enable fast scanning of the scattering phase function within a field of view of 55°. The full dynamic range of the detection system can be used by increasing the signal-to-noise ratio by means of averaging successive scans. The calibration of the angular response of the instrument is achieved by obtaining the transfer function of the optical detection system using Rayleigh scatterers. Accurate particle sizing of individual polystyrene spheres (ranging from 1.5 to 9 μm in diameter) in aqueous suspension is achieved by maximizing a correlation coefficient between precalculated tables of Mie phase functions and data obtained from the polar nephelometer. Good correlation is achieved between experimental and theoretical data, proving the functioning of the instrument as a fast and convenient particle sizer.

OCIS codes: 290.5820, 290.4020, 290.5850, 170.1530.

1. Introduction

Numerous types of polar nephelometer have been designed for obtaining the scattering phase function to infer size,[1–7] refractive index,[3,4,8] and internal structure[3,6,7] of scatterers. Modulation of the incident beam polarization state has also been incorporated in polar nephelometers[9,10] to increase information content in the measurement of the phase functions. Polarization measurements can be particularly useful in estimating molecular composition and microphysical parameters of the scatterers.[9–11] A concise description of the light scattering matrices, formulated in terms of Mueller matrices, was presented by Hunt and Huffman[12] for polar nephelometers.

Two main types of design of polar nephelometers can be differentiated: the first one uses a single detector adjustable to different angles, the second one measures simultaneously the light scattered at many angles with a set of multiple fixed detectors, positioned around the test space. The first type offers variable angular resolution[2,12] but is slow, whereas the second type has limited angular resolution but makes the measurement time almost instantaneously.[3,7,13] When a polar nephelometer is used for particle sizing by inversion of light scattering data using Mie theory, the angular resolution is particularly important, as the angular frequency of the oscillations in the scattering phase function of individual scatterers increases with particle size. Also, when characterizing polydisperse concentrations, the measurement time is crucial for the correct determination of the phase function, as the motion of scatterers should be very small with respect to the time it takes to scan the angular field of measurement.

The characterization of particle size distributions according to the National Institute of Standards and Technology (NIST) can be achieved using different techniques[14]: sieving (20 μm to 125 mm), gravitational sedimentation techniques (0.1 to 300 μm), optical light microscopy (1 μm and up), scanning electron microscopy (SEM) (0.1 to 1000 μm), transmission electron microscopy (TEM) (0.01 to 10 μm), and laser diffraction analysis (0.04 to 8000 μm).

All these techniques are well-known and are used systematically for the characterization of particle size distributions in laboratory and industry. Each method presents advantages and inconveniences, and each is used according to *a priori* known specifications of the sample to be characterized. SEM and TEM techniques require time-consuming sample preparation but do not need to refocus on each particle due to their depth of field, while optical light microscopy has the convenience of quick sample preparation but needs to have a proper focus for each particle under analysis. On the other hand, laser diffrac-

J.-L. Castagner (jlcastagner@hotmail.com) is with the Department of Biomedical Engineering and I. J. Bigio is with the Department of Biomedical Engineering, Department of Electrical and Computer Engineering, and the Boston University Photonics Center at Boston University, Boston, Massachusetts 02215.

Received 19 June 2006; revised 8 September 2006; accepted 13 September 2006; posted 22 September 2006 (Doc. ID 72093); published 17 January 2007.

0003-6935/07/040527-06$15.00/0

tion analysis can be used for dry powders, liquid suspensions, sprays, and emulsions but requires knowledge of the optical properties of the sample. This technique cannot differentiate between dispersed particles and agglomerates of particles.[14]

We presented, in a previous paper,[15] the proof of principle of a polar nephelometer for measuring the scattering phase function of particles in suspension, the design of which is based on a rotational confocal imaging setup. Fast measurements (<1 s) of the scattering phase function were obtained for scattering angles between 70° and 125°. In addition to the fast scanning capability of the instrument, averaging of successively acquired scans enables a many-fold increase in the signal-to-noise ratio to effect a large increase in the dynamic range of the detection system. Mie theory fits to the experimental data were found to be in good agreement for known particle sizes, but nevertheless some alignment and system calibration issues were yet to be resolved. Of major importance for the correct measurement of the phase function with this system was the determination of the optical detection system transfer function. Nonuniformity was observed in the angular response of the system to Rayleigh scatterers illuminated with *s*-polarized incident laser light at a wavelength of 633 nm, which (theoretically inferred from Mie theory calculations within the range of angles covered by the instrument) should be almost constant. Discrepancies between experimental data obtained with the instrument and Mie theory calculations with the mean diameter of the particle size distributions used were notable; however a significant correlation was clearly observed. We present the engineering improvements made to the previous prototype of the instrument, a simple calibration method, and provide data proving its function as a valid single particle sizer.

2. Methods

A full description of the basic principle of operation of the polar nephelometer was published previously.[15] Figure 1 shows the setup of the instrument. The instrument is based on confocal imaging of the test space through a range of scattering angles by means of a rotating mirror that deflects light scattered from the test space through a set of conjugated off-axis parabolic (OAP) mirrors. A laser beam at 632.8 nm passes through a linear polarizer and a half-wave plate successively. Polarization states orthogonal and parallel to the scattering plane (x, y), namely, s and p polarizations, are set by adjusting the half-wave plate. Particles illuminated by the laser beam that is focused at the center of the test space scatter light that is imaged on the face-centered rotating mirror that scans the field of view of the OAP mirrors. This light is then analyzed through the detection system that comprises a pinhole and an aperture placed at a distance $2f$ from the image relay lenses. The function of the pinhole is to limit the imaged width of the test space, while the slit aperture determines the angular resolution of the detector. In this way, fast scanning of the field of view of the system is achieved with minimal mechanical constraints.

A. Alignment

We pointed out in the initial publication on the instrument[15] some alignment issues such as the precision centering of the sample holder at the focus of the first parabola. This has been solved with a precision quartz tube that fits into a Teflon-coated aluminum guide to align it. The Teflon coating was used to avoid damaging the surface of the quartz tube when inserting and removing it. We also replaced the 1 in. (2.54 cm) OAP mirrors system by 2 in. (5 cm) diameter OAP mirrors, mounted on a right-angle bracket aluminum piece, allowing for symmetrical positioning of the OAP mirrors. In this way, the OAP mirrors optical alignment was more precisely controlled.

B. Rotating Mirror Position Readout

The angular position of the rotating mirror being a critical issue as well, we implemented an optical readout of the motor shaft position. The stability of the rotational speed of the motor is ~5%, which is slow compared to a single scan. Therefore its varia-

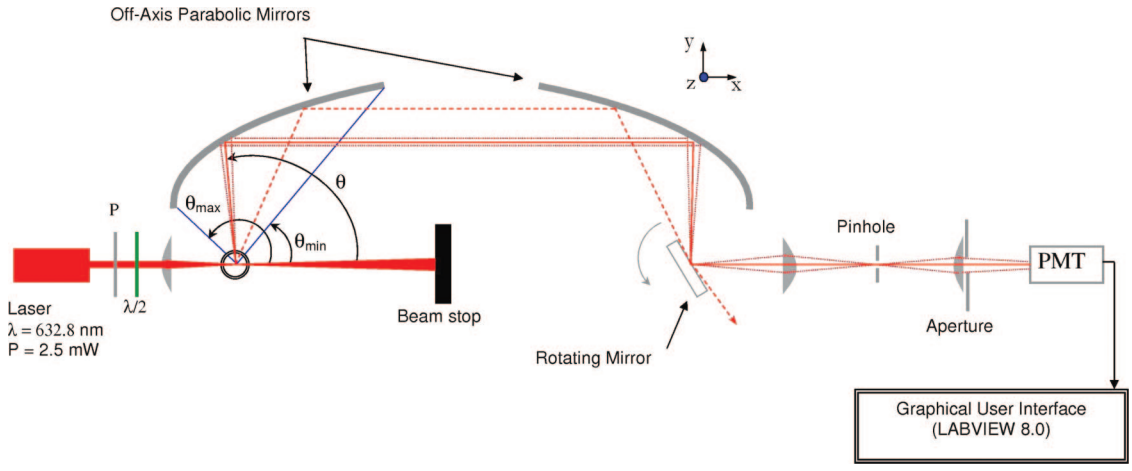

Fig. 1. (Color online) Schematic of the polar nephelometer.

tions over the angular range of measurements are not significant. Two optical pulses are generated when the mirror position is 0° and 35°, by means of a reference disk with two slits separated by 35°, which rotates between the emitter and the receiver diodes of an optical reader. Initial calibration of the absolute angular position of the mirror is achieved using a face-centered mirror mounted on a calibrated rotational mount at the focus of the first OAP mirror. The angular reference position of the mirror is obtained by sending the incident laser beam back upon itself (at 180°), then setting the calibration mirror at a known angle to produce a specific-angle signal at the detection side of the setup.

C. Data Acquisition System

We have improved the data acquisition system, which previously used a digital oscilloscope to perform the averaging of successive scans. Using a National Instruments data acquisition card driven by a LabVIEW 8.0 graphic user interface, the scattered light signal is sampled 1024 times per scan, with the trigger set at the half-height of the positive edge of the first position-reference pulse. The sampling frequency is adjusted so that the scattered light signal is contained between the two pulses. An interpolation scheme is applied to the scattered light intensity signal between the minimum and the maximum angles of interest to fit the same number of samples for each acquired scan, namely, 1024. In this way, small variations in the speed of the motor from one scan to the next do not affect the number of samples per scan. N successive scans are then acquired and successively averaged to increase the signal-to-noise ratio. N can be set to any integer value using the graphic user interface. In this way, flexibility in the setting of the instrument is achieved.

D. Calibration

Calibration of the angular intensity response of the instrument takes into account various effects: slight misalignment of the receiving optics (pinhole, focus of collecting lens); optical transfer function of the OAP mirrors; slight variations in the thickness of the quartz sample tube, etc. All these parameters can have an effect on the measured angular scattered light intensity distribution. To compensate, a simple procedure was designed, similar to earlier work in which Rayleigh scatterers were used to obtain absolute calibration of polar nephelometers with unpolarized light,[16] but different in that we need to calibrate the instrument only relatively. Small particles in suspension, of mean diameter 30 nm, were used to produce quasi-Rayleigh scattering. With a standard deviation of 18% for the diameter and a real refractive index of 1.58 for the particles, this size distribution remained within the Rayleigh range. This is well suited for the calibration, as the s-polarized scattered light intensity slowly varies only a few percent over the range of angles viewed by the system (70°–125°). Therefore light scattered from any particle within the size distribution had the same angular dynamic, but a different relative intensity due to size variation. The measured reference angular s-polarized scattered intensity distribution $I_{cal}{}^{s}(\theta)$ was recorded to obtain the optical transfer function $G(\theta)$ of the system:

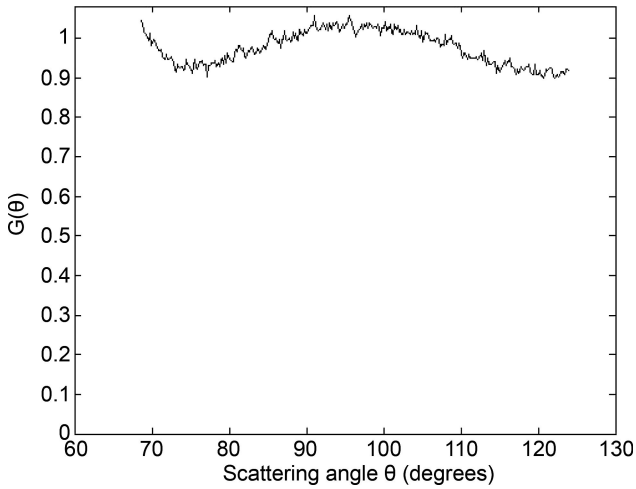

Fig. 2. Transfer function $G(\theta)$.

$$G(\theta) = \frac{I_{th}{}^{s}(\theta)}{I_{cal}{}^{s}(\theta)}, \tag{1}$$

where $I_{th}{}^{s}(\theta)$ is the calculated angular s-polarized phase function across the field of view of the system for a 30 nm diameter particle.

The calibrated measured angular s- or p-polarized angular scattered intensity distribution is then obtained according to

$$I^{s,p}(\theta) = G(\theta) I_{\exp}{}^{s,p}(\theta). \tag{2}$$

The system optical transfer function $G(\theta)$ is shown in Fig. 2. $I_{th}{}^{s,p}(\theta)$ and $I^{s,p}(\theta)$ are compared in Fig. 3. This demonstrates that the system transfer function is not polarization sensitive. Thus the s-polarization calibration can serve as the transfer function for both polarizations for this range of angles.

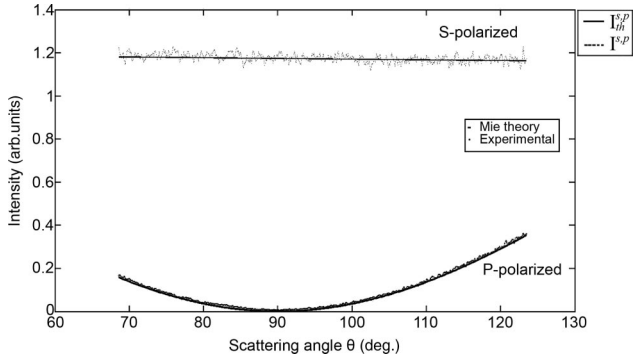

Fig. 3. Comparison between calibrated experimental data (dotted curve) and theoretical data (dashed curve).

Table 1. Manufacturer's Particle Size Distribution Specifications

	Sample Number				
	1	2	3	4	5
Mean diameter d_0 (μm)	1.5 ± 0.05	2.92 ± 0.005	5.030 ± 0.035	6.992 ± 0.050	8.957 ± 0.056
Standard deviation (μm)	0.07	0.09	0.05	0.07	0.09
NIST available	No	No	Yes	Yes	Yes

3. Measurements with Polystyrene Spheres

A. Particle Sizing Technique

A simple particle sizing technique was designed to rapidly obtain the size information from the angular scattered light intensity measured with the instrument. A similar procedure was carried out earlier in which size-separated particles were analyzed with a polar nephelometer to infer the refractive index using a Mie theory fitting process.[8] In our methodology, theoretical phase functions of both s and p polarizations were precalculated in tables as a function of the particle size diameter (increments of 30 nm), using Mie theory[17] with real refractive index values of 1.58 and 1.33 for the polystyrene spheres and water, respectively. A correlation coefficient was then calculated between the experimental data and each of the precalculated phase functions. The estimated particle diameter is determined by simply selecting the maximum correlation coefficient.

To validate the functioning of the polar nephelometer as a single particle sizer, we tested the system with five different particle size distributions, the specifications of which are summarized in Table 1. Figure 4 plots the measured angular scattered light intensities of s and p polarizations for sample 4 and the respective Mie theory fits. d_0 is the estimated diameter of the Mie theory fit.

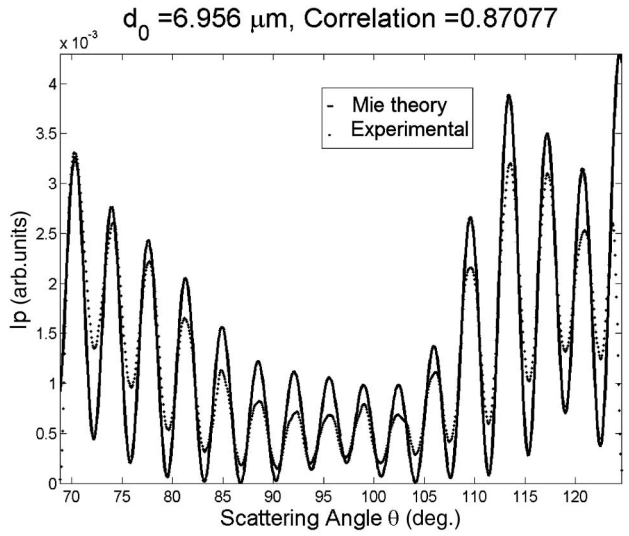

(a)

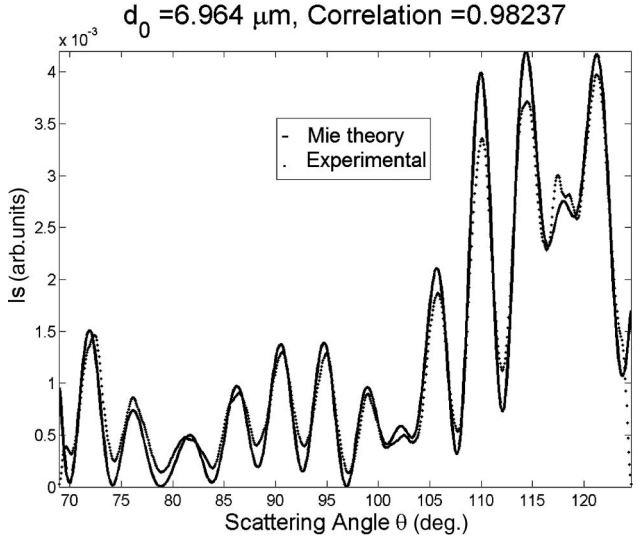

(b)

Fig. 4. (a) p- and (b) s-polarized intensity (dotted curves) fitted to Mie theory (solid curves). d_0 is the estimated particle diameter from the fit with $-1 <$ correlation < 1.

B. Measurements

For each sample, particles were suspended in water at low concentration, for which only single scattering events occurred within the measured volume. Twenty measurements of each sample were acquired with the nephelometer to constitute a significant statistical analysis. The mean diameter of each measured size distribution and its relative standard deviation is plotted in Fig. 5 with respect to the manufacturer spec-

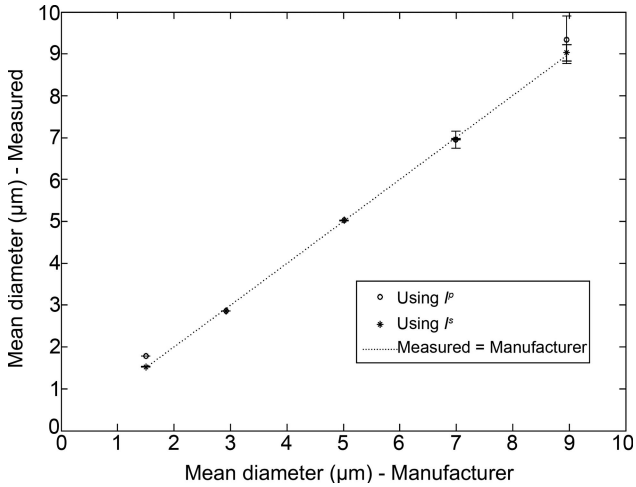

Fig. 5. Measured mean diameter versus manufacturer mean diameter. (○) Using I^p. (*) Using I^s.

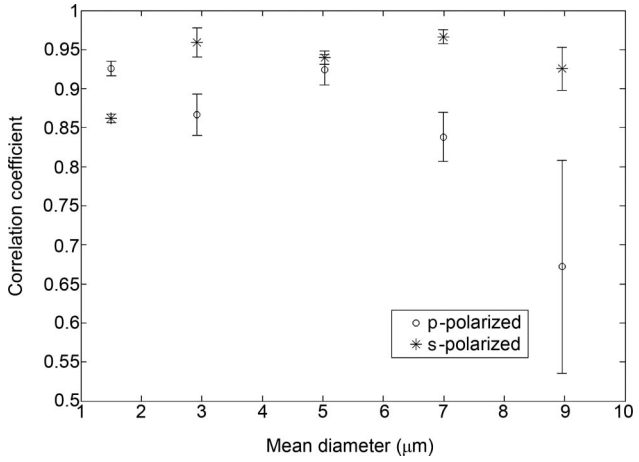

Fig. 6. Mean value and standard deviation of the correlation coefficient.

ifications. The dashed line represents the perfect correlation between them. The mean value and standard deviation of the correlation coefficient obtained for each data point is shown in Fig. 6. Measurements were obtained for both polarization states I^s and I^p.

4. Discussion

The calibration procedure presented in Section 2 takes into account the fact that small particles in the Rayleigh regime scatter almost isotropically for the range of angles of the instrument (70°–125°). Thus the *s*-polarized light scattered by these particles is particularly well-suited for obtaining the transfer function of the instrument, in a similar way that a Dirac function is often used to obtain the frequency response of various systems. If the range of angles of the instrument is different, the calibration can be carried out in a similar manner but with $I_{th}^s(\theta)$ set accordingly. It should be noted that problems would arise if the calibration were to be measured with *p*-polarized light from Rayleigh scatterers because Eq. (1) would create indeterminate numerical values for $G(\theta)$ around $\theta = 90°$ as $I_{th}^p(\theta)$ and $I_{cal}^p(\theta)$ would both have null values.

In Fig. 4 are presented typical results obtained for a particle size distribution with a mean centered at $\sim$7 μm. The oscillatory nature of the phase functions is clearly matched to Mie theory, with a correlation coefficient of 0.98 and 0.87 for *s* and *p* polarizations, respectively. A common problem in polar nephelometers and other laser-based systems (such as laser Doppler anemometry) is the intensity distribution of the incident laser beam. If illuminated with a nonuniform spatial intensity distribution, errors arise in the prediction of the phase functions when using Mie theory. This has been partially solved by the generalized Lorentz–Mie theory.[18] However, in our experiments we assumed the size of the scatterers to be significantly smaller than the width of the beam waist ($\approx$77 μm) and therefore used the simpler version of the Mie theory. We will explore, in the future, the implementation of the generalized Lorentz–Mie theory to increase the correlation between experimental data and theoretical predictions. Other potential causes that would reduce the correlation between measurements (Fig. 6) and Mie theory fits are slight nonsphericity in the calibrated spherical particles used and a lack of oscillatory behavior in the scattering phase function within the angular range of the instrument. Thus this technique is not suitable for sizing particles in the Rayleigh-scattering regime.

From Fig. 5, it appears that the polarization state affects the quality of the measurements, as all experimental data agree well with the manufacturer specifications with the exception of samples 1 and 5 for *p* polarization. The discrepancy between the measured mean diameter of sample 1 and the manufacturer's mean diameter is thought to be due to the inherent lack of significant oscillations in the *p*-polarized phase function within the angular range of the instrument, thereby diminishing the accuracy of the correlation–coefficient technique for this polarization state. The relatively large standard deviation of the size distribution obtained with sample 5 using *p*-polarized light is thought to be due to intrinsic errors in the determination of the correlation coefficient, caused by the specific shape of the oscillatory behavior of *p*-polarized light. Nevertheless, these errors were not present for *s*-polarization measurements.

From these measurements, it is shown that scattered light measurements of *s* polarization are more effective to provide accurate information for obtaining the size of individual spherical scatterers. We can also estimate the goodness of the Mie theory fit with the criterion correlation coefficient >0.8 when using *s* polarization for particle sizing (Fig. 6).

5. Conclusion

We have developed a single particle sizer based on the scattering phase function obtained with the polar nephelometer, which is fast and convenient for particles in suspension. Although its field of view was set to a range of 70°–125° for the scattering angle, the data obtained with the instrument were useful to measure individual particle sizes using a correlation coefficient technique that matches experimental data with precalculated Mie theory data of a specific polarization state. The results validate the functioning of this instrument as a single particle sizer. Additionally, the phase function from ensembles of particles, instead of a single particle, could also be measured. An appropriate inversion technique could then be used to retrieve the particle size distribution.

We used particles in suspension at low concentration in water, but the instrument should not be restrained to aqueous solutions. In fact, we believe the size retrieval would be more accurate for levitated particles or aerosols, as the system transfer function would not be affected by the sample glass tube imperfections.

We are currently conducting experiments with biological cells in suspension undergoing apoptosis to provide an optical signature of the apoptotic process.

We are also developing a version of the nephelometer that incorporates simultaneous measurements of the *s*- and *p*-polarization states in order to obtain additional information (shape, roughness) from individual scatterers.

This work is supported in part by the National Cancer Institute of the National Institutes of Health (grant U54 CA104677), and by the Boston University Photonics Center.

References

1. B. Steiner, B. Berge, R. Gausmann, J. Rohmann, and E. Rhl, "Fast *in situ* sizing technique for single levitated liquid aerosols," Appl. Opt. **38,** 1523–1529 (1999).
2. M. Z. Hansen and W. H. Evans, "Polar nephelometer for atmospheric particulate studies," Appl. Opt. **19,** 3389–3395 (1980).
3. Z. Ulanowski, R. S. Greenaway, P. H. Kaye, and I. K. Ludlow, "Laser diffractometer for single-particle scattering measurements," Meas. Sci. Technol. **13,** 292–296 (2002).
4. W. Kaller, "A newpolar nephelometer for measurement of atmospheric aerosols," J. Quant. Spectrosc. Radiat. Transfer **87,** 107–117 (2004).
5. S. Hochrainer, "Further developments of the particle counter sizer PCS-2000," J. Aerosol Sci. **31,** Suppl. I, S771–S772 (2000).
6. O. Crepel, J.-F. Gayet, J.-F. Fournol, and S. Oshchepkov, "A new airborne polar nephelometer for the measurements of optical and microphysical cloud properties. Part I: Theoretical design," Ann. Geophys. **15,** 451–459 (1997).
7. O. Crepel, J.-F. Gayet, J.-F. Fournol, and S. Oshchepkov, "A new airborne polar nephelometer for the measurements of optical and microphysical cloud properties. Part II: Preliminary tests," Ann. Geophys. **15,** 460–470 (1997).
8. A. Mennella and F. Prodi, "Optical characterization of size separated aerosol particles of different composition and morphology with a polar nephelometer," Pure Appl. Opt. **2,** 471–488 (1993).
9. D. Miller, M. S. Quinby-Hunt, and A. J. Hunt, "Novel bistatic polarization nephelometer for probing scattering through a planar interface," Rev. Sci. Instrum. **67,** 2089–2095 (1996).
10. D. Banfield, P. Gierasch, M. Roos-Serote, D. Stam, H. Volten, O. Munoz, M. Mishchenko, and R. Dissly, "Planetary polarization nephelometer," in *Workshop Proceedings of the International Planetary Probe Atmospheric Entry and Descent Trajectory Analysis and Science,* A. Wilson, ed. (European Space Agency, 2004).
11. D. Banfield, P. Gierasch, and R. Dissly, "Planetary descent probes: polarization nephelometer and hydrogen ortho/para instruments," in *Aerospace, 2005 IEEE Conference,* (IEEE, 2005), pp. 1–7.
12. A. J. Hunt and D. R. Huffman, "A new polarization modulated light scattering instrument," Rev. Sci. Instrum. **44,** 1753–1762 (1973).
13. W. Kaller, "A new polar nephelometer for measurement of atmospheric aerosols," J. Quant. Spectrosc. Radiat. Transfer **87,** 107–117 (2004).
14. A. Jillavenkatesa, S. J. Dapkunas, and L. S. H. Lum, *Particle Size Characterization,* NIST (Natl. Inst. Stand. Technol.) Spec. Publ. 960-1 (2001).
15. J.-L. Castagner and I. J. Bigio, "Polar nephelometer based on a rotational confocal imaging setup," Appl. Opt. **45,** 2232–2239 (2006).
16. B. R. Jennings and H. Plummer, "Light-scattering photometer calibration," J. Phys. D **1,** 1201–1209 (1968).
17. C. Bohren and D. Huffman, *Absorption and Scattering of Light by Small Particles* (Wiley-Interscience, 1983).
18. B. Maheu, G. Grehan, and G. Gouesbet, "Diffusion de la lumiere par une sphere dans le cas d'un faisceau d'extension finie—1. Théorie de lorenz-mie generalisee: les coefficients g_n et leur calcul numerique," J. Aerosol Sci. **19,** 47–53 (1988).